Journal of Materials Chemistry C

Accepted Manuscript

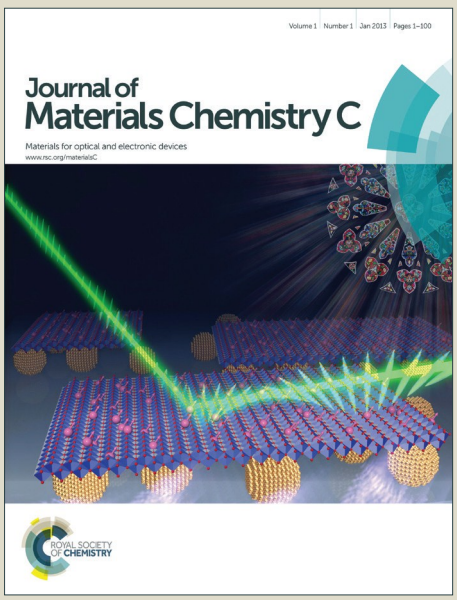

ROYAL SOCIETY OF CHEMISTRY

www.rsc.org/materialsC

Laser Induced Photothermal Effect in InAs Nanowire: Tuning Hole Density

Dipanwita Majumdar,[1] Daniele Ercolani, [2] Lucia Sorba, [2] and Achintya Singha[1*]

[1]Department of Physics, Bose Institute, 93/1, Acharya Prafulla Chandra Road, Kolkata 700 009, India

[2]NEST, Istituto Nanoscienze-CNR and Scuola Normale Superiore, Piazza S. Silvestro 12, I-56127 Pisa, Italy

[*] Author to whom correspondence should be addressed. Electronic mail: achintya@jcbose.ac.in

Phone: + 91 33 23031177, Fax: + 91 33 23506790

Abstract

Optical control of hole density in InAs nanowire is achieved by simultaneous photogeneration and local heating, varying the laser power during Raman measurements. We have derived the laser induced temperature rise from the Raman line-shape analysis. As a result of laser heating, an oxide layer is formed on the surface of the nanowire, which acts as a "photogating layer" (PGL). Upon light illumination, photogenerated electrons trapped in the PGL form a built-in electric field to deplete the free electrons in the InAs core, thus the hole density increases in the InAs with the increase of laser induced photothermal effect. This phenomenon is demonstrated by monitoring the coupled hole plasmon-LO phonon (CPLP) mode. The values of hole density have been estimated from a full line-shape analysis of the measured Raman spectra at different laser powers. Our study shows a significant correlation between oxide layer thickness and hole density. These findings open an optical way to the simultaneous manipulation and monitoring of the carrier density in nanowires.

1. Introduction

Semiconductor nanowires (NWs) have been intensively studied in the last decade due to their novel physical properties and potential applications in the new generation of extraordinary tiny devices [1,2] Among various III-V semiconductors, having a narrow band gap, considerable research attentions have particularly been paid to InAs as they possess unusually high charge mobility due to small electron effective mass. At room temperature, bulk InAs has a band gap of 0.354 eV and an effective mass ~ 2.4 $\times 10^{-3}$, giving rise to electron mobility of 3×10^{4} cm^2 V^{-1} s^{-1}.[3-7] Owing to these features, InAs has been considered as a suitable material for making high-performance nano-electronic and nanophotonic devices.[8-15] However, tuning the performances of such nano-devices is another challenge aside from the fabrication of these objects. In InAs NW, the diameter dependent metal-semiconductor contact properties [16,17] and crystal structure-dependent piezoelectric and piezoresistive effects have been investigated.[18] In NWs as the surface to volume ratio is large, the surface charge concentration and surface defect states play a significant role in their electronic properties. Particularly, InAs NWs are very sensitive to the surface properties; therefore, it can be used as an efficient sensor for chemical molecules.[19,5] Recently, Guo *et al.* and Miao *et al.* have explored the effects of atmospheric molecules on the photoresponse of InAs based photodetectors.[19,5] The defect states on the surface of an n-type InAs NWs act as "photogating layer" (PGL). Upon light irradiation, the photogenerated electrons in InAs are trapped in PGL leaving unpaired holes, which modulate the photoresponse.[19] However, to the best of our knowledge, no optical technique for simultaneous tuning and monitoring of the carrier density in InAs NWs has been reported. Recently, in III-V nanostructures an optical method has been applied successfully to control and monitor electron population with single electron accuracy.[20,21]

In this work, we study the tuning of hole density in InAs NWs by the photothermal effect. Micro-Raman spectroscopy is an amenable optical technique for such studies because of the following three reasons: First, laser light from a Raman setup creates electron and hole pairs. Second, an intensely focused laser beam provides energy that can substantially increase the local temperature,[22-30] which can modify the surface of the NW. [28-30] Third, in polar semiconductors (III-V compound) having sufficient carrier density, the frequency of the free carrier plasmon is comparable to the optical frequency. The interaction between the electronic dipole moment associated with the longitudinal optical (LO) phonons and the electric field connected to the carrier plasmons gives a new excitation having coupled plasmon-phonon character.[31-37] The frequency of the new mode is different from LO phonon and plasmon frequency and it is a function of carrier density. The new mode is defined as coupled plasmon-LO phonon (CPLP) mode.[34,35] In p-type doped polar semiconductors, the interaction between hole plasmon and LO phonon leads to the formation of CPLP mode.[34,35] Unlike p-doped semiconductor, a significant amount of holes created by photo irradiation can produce CPLP mode only if the photogenerated electrons are trapped within the system.[38] The CPLP mode is Raman active and the spectral width plus the position of the mode is sensitive to the hole density.[34,35,39] Therefore, the temperature of a NW can be raised as well as the effect of photogenerated charge carriers can be simultaneously monitored from the CPLP mode during Raman measurements. From the Raman response of the InAs NW, it is found that the hole density increases with the rise in laser power. We have correlated the hole density with oxide layer thickness, formed on the surface of the NW due to laser induced heating.

2. Experimental Section

Aligned InAs NWs were grown on an InAs (111)B substrate using chemical beam epitaxy at 425± 10 ^{o}C, with metal organic line pressure of 0.3 and 1.0 Torr for trimetyl indium and tertiarybutyl arsine, respectively. The details of growth procedure can be found elsewhere.[40] The unintentionally incorporated oxygen atoms during the growth always tend to stay at the lateral surfaces of InAs nanowires.[41] The resulting NWs have polytype phase where zinc blende phase is present as a staking fault in wurtzite structure with average length and diameter of ~1μm and 40 nm respectively, as confirmed by electron microscopy characterization.[42,43]

Raman measurements were performed in backscattering geometry using LabRAM HR (Jobin Yvon) spectrometer equipped with an air-cooled argon ion (Ar^{+}) laser of wavelength 488 nm and a Peltier-cooled charge-coupled-device (CCD) detector. For Raman measurements InAs NW was transferred on a silicon (Si) wafer, with the NW axis laying parallel to the Si surface. The laser beam from the Raman spectrometer was tightly focused (beam diameter ~661 nm) onto the NW through a 100X microscope objective with numerical aperture (NA) 0.9. For efficient heating the laser polarization was aligned along the axis of the NW.[44] Before acquisition of the Raman spectrum at a laser power, the NW was exposed with the same laser power for 5 minutes. The Raman measurements at vacuum were performed using Linkam stage (model: THMS 600). All spectra were collected at similar experimental conditions at different laser powers. Since the thermal anchoring between NW and the wafer is not very good, a substantial amount of heat is conserved locally in the NW.

2. Results and Discussion

Figure 1 shows selected Raman spectra of InAs NW irradiated with different laser powers for the same length of time. The laser power employed here ranges from 0.05 mW

(1.46×10^8 W/m^2) to 9.10 mW (2.65×10^{10} W/m^2). The peaks observed around 216.6, 231.2 and 239.6 cm^{-1} can be attributed to the transverse optical (TO), surface optical (SO) and longitudinal optical (LO) phonon modes, respectively.[42] Beside the TO, SO and LO phonon modes, after a certain laser power a new peak, termed CPLP, develops at the lower shoulder of the LO mode, which shifts towards TO with the increase of laser power.

The Raman spectra were fitted with multi-Lorentzian line-shapes in the range from 200 to 250 cm^{-1} to account for TO, SO, LO and CPLP modes. The fitted spectrum at 8.74 mW laser power is displayed in the inset of Figure 1. Some selected fitted spectra, acquired at other laser powers are shown in the Figure S1 in the Supplementary Material. The Raman modes show downshift in energy as well as an increase in full width at half maxima (FWHM) with the increase of laser power. The possible reasons for the downshift and linewidth broadening are the phonon confinement and laser induced heating effects. The confinement effect cannot explain these observations as the diameter of our NW is 40 nm.[45] Thermal anharmonicity effect caused by temperature change become prominent at higher temperatures due to the larger extent of lattice vibrations and induces both linewidth broadening and downshift of the phonon modes.

An intense focusing of the laser beam in micro-Raman setup can lead to significant heating of the sample. From the FWHM of the LO modes at different laser powers, as shown in Figure 2(a), the rise in temperature with laser power can be calculated using Equation1.[46]

$$\Gamma(T) = \Gamma_0[1 + \frac{2}{e^{\hbar\omega_0/2k_BT} - 1}] \qquad (1)$$

where Γ_0 is the FWHM and ω_0 is the Raman frequency at 0 K. Figure 2 (b) displays the change in temperature as a function of laser power, which shows an increasing trend of temperature with laser power.

Figure 3(a) shows the intensity ratio between CPLP and LO modes as a function of laser power. The ratio increases with the rise of laser power, which can be attributed to the interplay between optical phonons and photogenerated charge carriers.

To explain the phenomena we propose a mechanism here. The incident photons generate electron-hole pairs in the NW and at the same time laser induced heat forms oxide layer on the surface of the NW. In III-V semiconductor at elevated temperature, the partial vapor pressure of group V elements is much higher than the group III elements.[47] Therefore, at higher temperature the group V elements evaporate easily from III-V semiconductors.[48] Furthermore, based on experimental studies, it is also reported that in InAs semiconductor at high temperature, the As atoms evaporate from the surface leaving In component behind.[49-52] Thus, the In_2O_3 is formed at the surface of the InAs NW due to the laser induced heating. During the formation of In_2O_3 layer, oxygen vacancy related defect states are formed, which act as acceptor and for charge neutrality it traps the photogenerated electrons in the InAs region, leaving unpaired holes inside the InAs core.[19,53,54] Thus, the oxide layer acts as a PGL. The whole process has been shown schematically in Figure 3(b). Upon light illumination, initially the photogenerated holes recombine with the background electrons in InAs.[5,19] So, the CPLP mode is not visible at the lowest laser power. But, with the increase of laser power the photogenerated electron-hole numbers increases and simultaneously, defect states also increase at the surface of the NW. As a result, more and more electrons are trapped at the surface that generate a strong built-in electric field, which further depletes the free electrons in the InAs core through capacitive coupling.[19] This whole process results in the increase of hole density inside the core. The CPLP mode, which reflects the interactions between these holes and LO phonons, is shown as shaded peak in the inset of Figure 1 and Figure S1 (in the Supplementary Material).

The formation of the In_2O_3 layer is confirmed from the appearance of Raman modes at 108 and 132 cm^{-1} [55] as shown in Figure 1. An absence of any As related mode in the measured Raman spectra implies that the As atoms sublime away. [28-30] The oxide layer on the surface of the NW gives rise to a core/shell structure having InAs for 0<r<a, In_2O_3 for a<r<b and air for r>b, as shown in the inset of Figure 3 (c). We have determined the morphological structure of the core/shell NW by monitoring the evolution of the SO phonon mode at different laser powers. The SO phonon mode appears due to different dielectric constant at the interface. SO phonons at the interface of the core/shell structure have been studied using a phenomenological continuum model in cylindrical core/shell geometry.[56] In this model, SO phonon dispersion equation is

$$(\varepsilon^{(1)}(\omega)-\varepsilon^{(2)}(\omega))(\varepsilon_D-\varepsilon^{(2)}(\omega))-(\varepsilon^{(1)}(\omega)+\varepsilon^{(2)}(\omega))(\varepsilon_D+\varepsilon^{(2)}(\omega))\gamma^{2n}=0 \qquad (2)$$

where, γ (=*b/a)* is the ratio between shell radius and core radius and ε_D is the medium dielectric constant (for r>b). The dielectric functions $\varepsilon^{(1)}(\omega)$ and $\varepsilon^{(2)}(\omega)$ for materials "1" and "2" are given by

$$\varepsilon^{(i)}(\omega)=\varepsilon_\infty^{(i)}\frac{\omega_{SO}^2-\omega_{iLO}^2}{\omega_{SO}^2-\omega_{iTO}^2} \quad with\ i=1,2 \qquad (3)$$

where $\varepsilon_\infty^{(i)}$ is the high frequency dielectric constant, ω_{iLO} and ω_{iTO} are the bulk longitudinal and transversal polar optical phonon frequencies at the Γ point for each material (i=1,2). The Equation 2 gives the SO phonon frequencies as a function of the parameter γ for different values of n (n=0,1,2,…).

To obtain an assessment of the NW thickness reduction with the increase in laser power, we calculate the values of γ solving Equation 3; using Equation 2 and the fitted parameters of the Raman spectra acquired at different laser powers. The following values are used for the calculation: static dielectric constant for indium oxide $\varepsilon^{(2)}(\omega)$=9.05,[57] and high frequency

dielectric constant of indium arsenide $\varepsilon_{\infty}^{(1)}(\omega)$=8.7.[58] The surrounding medium of the NW is a mixture of air and silicon substrate. The effective dielectric constant of the surrounding medium is taken as 3.14. Figure 3(c) shows that the *b/a* ratio increases with the increase of laser power, indicating an increase in oxide layer thickness. This result is also reflected in the Raman profile, where the In_2O_3 peaks become more and more prominent with increasing laser power (see Figure S2 in the Supplementary Material).

As mentioned above, with increasing oxide volume more and more electrons are trapped, which strengthen the built-in electric field. As a result, the net hole density increases within the non-oxidized NW, which has been confirmed using a model proposed by Ruppin and Englman.[59] According to this model, the relation between the SO and TO phonon modes can be expressed by

$$\omega_{SO}^2 - \omega_{TO}^2 = \frac{\omega_P^2}{\varepsilon_{\infty}^{(1)} + \varepsilon^{(2)}(\omega).\rho} \qquad (4)$$

where ω_P is the screened ion plasma frequency and ρ can be expressed as:

$$\rho = \frac{K_1(x)I_0(x)}{K_0(x)I_1(x)} \qquad (5)$$

where $K_n(x)$ and $I_n(x)$ are the modified Bessel functions and $x=qr$ (r being the radius of the NW and the value of q for 488 nm excitation is $4\pi/\lambda$=0.026 cm^{-1}). The plasmon frequency ω_P can be related to the free carrier concentration (n_h) and effective hole mass of InAs (m^*=0.41m_e) [60] by [59]

$$\omega_P^2 = \frac{\pi n e^2}{\varepsilon_{\infty} m^*} \qquad (6)$$

Columns 2 and 3 of Table 1 summarize the values of r and the corresponding values of x for different laser powers, respectively. Using the values of ω_{TO} and ω_{SO} from the deconvoluted experimental Raman spectra we have calculated ω_P^2, which is listed in column 4. Finally, we

have calculated hole density n_h for different laser powers using Equation 6 (last column). The hole density n_h increases by almost an order of magnitude with laser power, which is consistent with the proposed model.

To further confirm the role of the oxide layer in increasing the hole density we have performed two sets of experiments. Firstly, the Raman measurements were performed using very low laser power to avoid laser induced heating on a NW before and after oxidation. The Raman spectrum of the NW without oxide layer is presented in the bottom of Figure 4 (black curve). The spectrum is well fitted with three Lorentzian corresponding to TO, SO and LO modes. As expected, the peaks related to the In_2O_3 are not visible (see the black curve in the inset of Figure 4). After the Raman measurement, the NW was irradiated by high laser power for the formation of an oxide layer on the surface of the NW. After some time, again Raman measurement was carried out at the same low laser power used for the measurement before irradiation and the measured spectrum is displayed as an orange curve in Figure 4. The peaks from the In_2O_3 are visible here (orange curve in the inset of Figure 4). After careful analysis of the spectrum within the range 200 to 250 cm^{-1}, we can clearly see the signature of CPLP mode. These results indicate that the presence of oxide layer on the surface of the NW is necessary to create hole plasmon in the InAs core , which generates CPLP mode.

Secondly, the power dependent Raman measurements were performed in vacuum (at 10^{-3} mbar). The obtained data are displayed in Figure 5. The spectra do not show In_2O_3 related any peak, which indicates that in the absence of O_2, the oxide layer is not formed on the surface of the NW. The CPLP mode is not also developed, which is very clear in the fitted spectra shown in Figure S3 in the Supplementary Material, where the spectra are well fitted with TO, SO and LO peaks in all powers. Here, the absence of CPLP mode is due to the absence of oxide layer. Therefore,

both the experiments confirm that the photogenerated electron-hole pairs are decoupled by trapping electrons in the In_2O_3 layer. Thus, the photothermal effect due to laser irradiation increases the photogenerated hole concentration in an InAs NW.

3. Conclusion

In conclusion, we have investigated the feasibility of using a focused laser beam to tune the electronic properties of an InAs NW. The collected Raman spectra at different laser powers are well modeled taking into account the TO, SO, LO and phonon like coupled mode of hole plasmon and LO phonon. The laser induced local temperature has been calculated using FWHM of LO phonon mode at different laser powers. We have estimated the thickness of the oxide layer formed by laser induced heating in air using DCA theory for cylindrical core/shell structure. The hole density has been determined using Ruppin and Englman model. Our study based on Raman spectroscopy, gives a good correlation between oxide layer thickness and hole density. Overall, these experiments show the charge tunability by photogeneration that allows to obtain NWs with a controlled concentration of holes.

Supporting Information

Electronic Supplementary Information (ESI) available: Raman spectra fitted with multiple Lorentzian functions at different laser powers taken in air and vacuum. Integrated intensity of the Raman modes of In_2O_3 as a function of laser power.

References:

1 W. Lu and C. M. Lieber, *Nat. Mater.* 2007, **6**, 841.

2 S. W Chung, J. Y. Yu and J. R. Heath, *Appl. Phys. Lett.* 2000, **76**, 2068.

3 S. Adachi, in Properties of Group-IV, III-V and II-VI Semiconductors (*Wiley*, 2005).

4 T. Takahashi, K. Takei , E. Adabi , Z. Y. Fan, A. M. Niknejad and A. Javey , *ACS Nano* 2010,**4**, 5855.

5 J. Miao , W. Hu, N. Guo , Z. Lu , X. Zou , L. Liao , S. Shi , P. Chen , Z. Fan , J. C. Ho , T.-X. Li , X. S. Chen and W. Lu , *ACS Nano* 2014, **8** , 3628.

6 S. A. Dayeh , D. P. R. Aplin , X. T. Zhou , P. K. L. Yu , E. T. Yu and D. L. Wang , *Small* 2007, **3**, 326.

7 Q. Hang, F. Wang, P. D. Carpenter , D. Zemlyanov, D. Zakharov, E. A. Stach , W. E. Buhro and D. B. Janes, *Nano Lett.* 2008, **8**, 49.

8 W. Wei, X. Y. Bao, C. Soci, Y. Ding, Z.-L. Wang and D. Wang, *Nano Lett.*2009, **9**, 2926.

9 M. Paladugu, J. Zou, G. J. Auchterlonie, Y. N. Guo, Y. Kim, H. J. Joyce, Q. Gao, H. H.Tan and C. Jagadish, *Appl. Phys. Lett.* 2007, **91**, 133115.

10 P. Krogstrup, J. Yamasaki, C. B. Sørensen, E. Johnson, J. B. Wagner, R. Pennington, M. Aagesen, N. Tanaka and J.Nygard, *Nano Lett.* 2009,***9***, 3689.

11 F. Zhou, A. L. Moore, J. Bolinsson, A. Persson, L. Fröberg, M. T. Pettes, H. Kong, L. Rabenberg, P. Caroff, D. A. Stewart, N. Mingo, K. A. Dick, L. Samuelson, H. Linke and L. Shi, *Phys. Rev. B* 2011, **83**, 205416.

12 O. Madelung, Semiconductors: Data Handbook (*Springer, Berlin*, 2004).

13 X. Y. Gong, H. Kan, T. Makino, T. Yamaguchi, T. Nakatskasa, M. Kumagawa, N. L. Rowell, A. Wang and R. Rinfret, *Cryst. Res. Technol.* 1995, **30**, 603.

14 R. V. Shenoi, R. S. Attaluri, A. Siroya, J. Shao, Y. D. Sharma, A. Stintz, T. E Vandervelde and S. Krishna, *J. Vac. Sci. Technol. B* 2008**, 26**, 1136.

15 S. Mou, A. Petschke, Q. Lou, S. L. Chuang, J. V. Li and C. J. Hill, *Appl. Phys. Lett.* 2008*,* **92***,* 153505.

16 T. Shi, M. Fu, D. Pan, Y. Guo, J. Zhao and Q. Chen, *Nanotechnology* 2015, **26**, 175202.

17 M. Q. Fu, D. Pan, Y. J. Yang, T. W. Shi, Z. Y. Zhang, J. H. Zhao, H. Q. Xu and Q. Chen, *Appl. Phys. Lett.* 2014, **105**, 143101.

18 X. Li , X. Wei, T. Xu , D. Pan , J. Zhao and Q. Chen, *Adv. Mater.* 2015, **27**, 2852.

19 N. Guo, W. Hu , L. Liao, S. P. Yip , J. C. Ho , J. Miao , Z. Zhang , J. Zou , T. Jiang , S. Wu, X. Chen and W. Lu, *Adv. Mater.* 2014, **26**, 8203.

20 S. Kalliakos, V. Pellegrini, C. P. Garcia, A. Pinczuk, L. N. Pfeiffer and K. W. West, *Nano Lett.* 2008*,* **8**, 577.

21 A. Singha, V. Pellegrini, A. Pinczuk, L. N. Pfeiffer, K. W. West and M. Rontani, *Phys. Rev. Lett.* 2010**, 104***,* 246802.

22 R. Jalilian, G. U. Sumanasekera, H. Chandrasekharan, and M. K. Sunkara, *Phys. Rev. B* 2006**, 74**, 155421.

23 A. Duzynska, J. Judek and M. Zdrojek, *Appl. Phys. Lett.* 2014**, 105,** 213105.

24 A. Taube, J. Judek, C. Jastrzębski, A. Duzynska, K. Świtkowski and M. Zdrojek, *ACS Appl. Mater. Interfaces* 2014*,* **6**, 8959.

25 R. Gupta, Q. Xiong, C. K. Adu, U. J. Kim and P. C. Eklund, *Nano Letters*, 2003, **3**, 627.

26 P. B. Roder, P. J. Pauzauskie and E. J. Davis, *Langmuir* 2012, **28**, 16177.

27 P. B. Roder, B. E. Smith, E. J. Davis, P. J. Pauzauskie and *J. Phys. Chem. C* 2014, **118**, 1407.

28 S. Yazji, I. Zardo, M. Soini, P. Postorino, A. F. i Morral and G. Abstreiter, *Nanotechnology* 2011, **22,** 325701.

29 S. Pal, R. Aggarwal, V. K. Gupta and A. Ingale, *Appl. Phys. Lett.* 2014,**105**,012110.

30 J. He, P. Chen, W. Lu, N. Dai and D. M. Zhu, *Appl Phys A* 2014, **115**, 885.

31 B. B. Varga, *Phys. Rev.* 1965, **137,** A1896.

32 K. S. Singwi and M. P.Tosi, *Phys. Rev.* 1966, **147,** 658.

33 C. G. Olson, D. W. Lynch and *Phys. Rev.* 1969, **177,** 1231.

34 G. Irmer, M. Wenzel and J. Monecke, *Phys. Rev. B* 1997, **56**, 9524.

35 G. Abstreiter, M. Cardona and A. Pinczuk, in Light scattering in solids IV, edited by Cardona, M.; Güntherodth, G.; (Springer, Berlin, 1984), p. 5.

36 B. Ketterer, J.Arbiol and A. F. i Morral, *Phys. Rev. B* 2011, **83**, 245327.

37 K. Jeganathan, R. K. Debnath, R. Meijers, T. Stoica, R. Calarco, D. Grützmacher and H. Lüth, *J. Appl. Phys.* 2009, **105**, 123707.

38 T. A. El-Brolossy and H. Talaat, *J. Raman Spectrosc.* 2008, **39**, 91.

39 W. Limmer, M. Glunk, S. Mascheck, A. Koeder, D. Klarer, W. Schoch, K. Thonke, R. Sauer and A. Waag, *Phys. Rev. B* 2002, **66**, 205209.

40 L. Viti, M. S.Vitiello, D. Ercolani, L. Sorba and A.Tredicucci, *Nanoscale Res. Lett.* 2012, **7**, 159.

41 M. Galicka, R. Buczko and P. Kacman, *J. Phys. Chem. C* 2013, **117**, 20361.

42 D. Majumdar, A. Basu, G. D. Mukherjee, D. Ercolani, L. Sorba and A. Singha, *Nanotechnology* 2014, **25,** 465704.

43 J. K. Panda, A. Roy, A. Singha, M. Gemmi, D. Ercolani, V. Pellegrini, L. Sorba, *Appl. Phys. Lett.* 2012, **100**, 143101.

44 C.C. Chang, H. Chen, C.C. Chen, W. H. Hung, I. K. Hsu, J. Theiss, C. Zhou and S. B. Cronin, *Nanotechnology* 2011, **22**, 305709.

45 T. Li, Y. Chen, W. Lei, X. Zhou, S. Luo, Y. Hu, L.Wang, T. Yang, and Z. Wang, *Nanoscale Research Letters* 2011, ***6,*** 463.

46 M. S. Liu, L. A. Bursill, S. Prawer and K. W. Nugent, *Appl. Phys. Lett.* 1999, **74,** 3125.

47 H. Morota and S. Adachi, *J. Appl. Phys.*2009, **105**, 043508.

48 S. J. Pearton and C. R. Abernathy, F. Ren, Topics in growth and device processing of III-V semiconductors (World Scientific, 1996).

49 P. K. Kashkarov, V. Y.Timoshenko, N. G. Chechenin and A. N. Obraztsov, *Laser Phys.* 1992, **2***,* 790.

50 R. Tsu, J. E. Baglin, G. J. Lasher and J. C. Tsang, *Appl. Phys. Lett.* 1979, **34,** 153.

51 T. E. Haynes, W. K. Chu, T. L. Aselage and S. T. Picraux, *J. Appl. Phys***.**1988, **63**, 1168.

52 J. He, P. Chen, W. Lu, N. Dai and D. M. Zhu, *J. Appl. Phys***.** 2012, **111**, 094316.

53 I. Hamberg and C.G. Granqvist, *J. Appl. Phys.* 1986, **60**, R123.

54 N. Han, F. Wang, J. J. Hou, F. Xiu, S. P. Yip, A. T. Hui, T. F. Hung and J. C. Ho, *ACS NANO* 2012, ***6,*** 4428.

55 H. S. Kim, H. G. Na, J. C. Yang, C. Lee and H. W. Kim, *Acta Physica Polonica A* 2011, **119***,* 143.

56 D. G.S. Pérez, C. T. Giner, R. P. Álvarez and L. Chico, *Physica E* 2014, **56,** 151.

57 A. Walsh, C. R. A. Catlow, A. A. Sokol and S. M. Woodley, *Chem. Mater.*2009, **21**, 4962.

58 H. Arabshahi, M. R. Khalvati and M. R. R. Abadi, *Brazilian Journal of Physics.*2008, **38**, 293.

59 R. Ruppin and R. Englman, Optical phonons of small crystals. *Rep. Prog. Phys.* 1970, **33,**149.

60 C. Kittel, Introduction to Solid State Physics, 5th edn., *Wiley, New York*, 1976

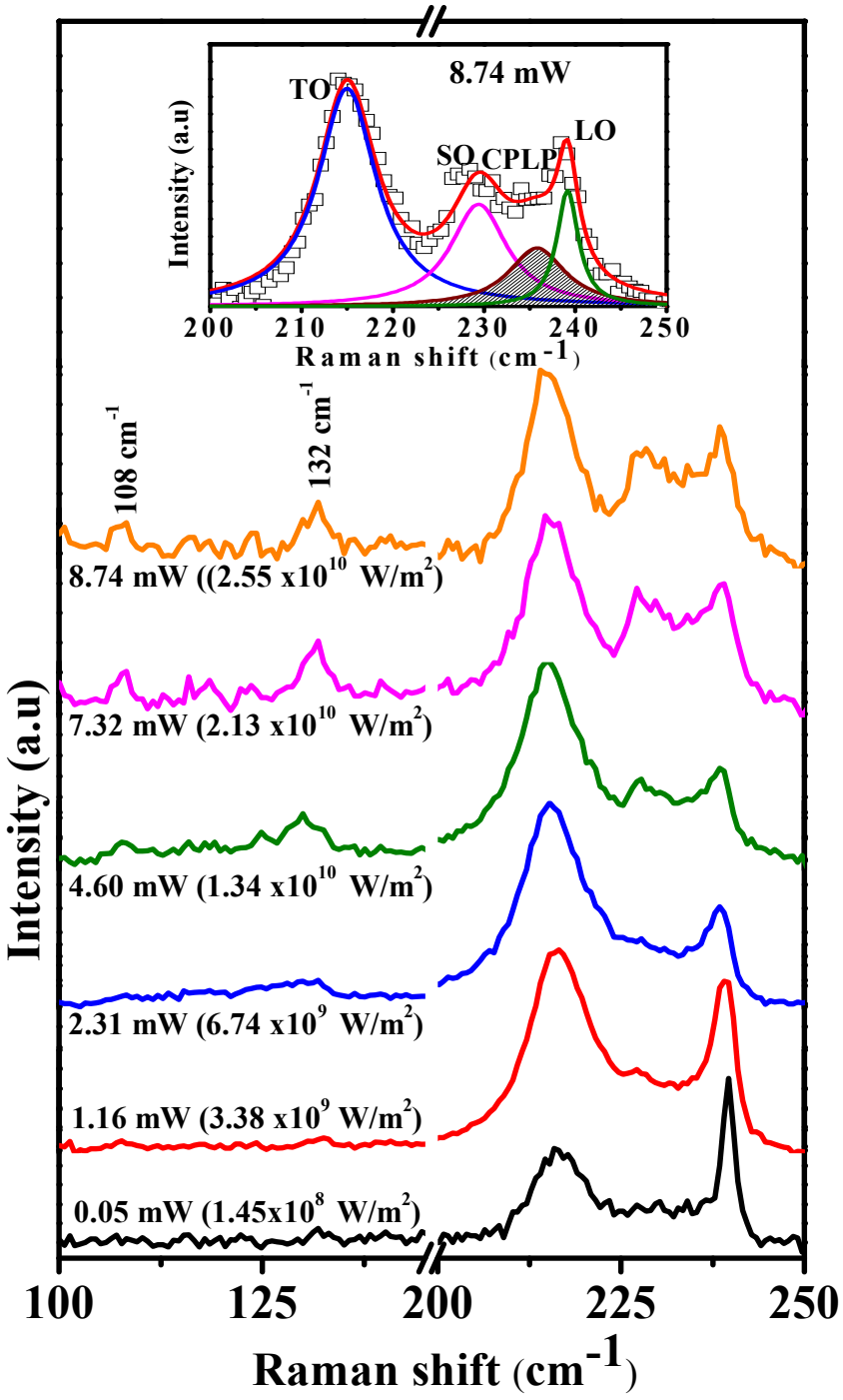

Figure 1: Raman spectra of InAs NW at different laser powers from lower (bottom) to higher (top) laser power (power density), indicated for each curve. The individual spectra are vertically shifted for clarity. The inset shows the Raman spectrum (symbols) at 8.74 mW laser power fitted with multiple Lorentzian functions. The red line is the result of multi- Lorentzian fit. The blue, magenta and green lines correspond to TO, SO and LO phonon modes, respectively. The shaded peak corresponds to CPLP mode.

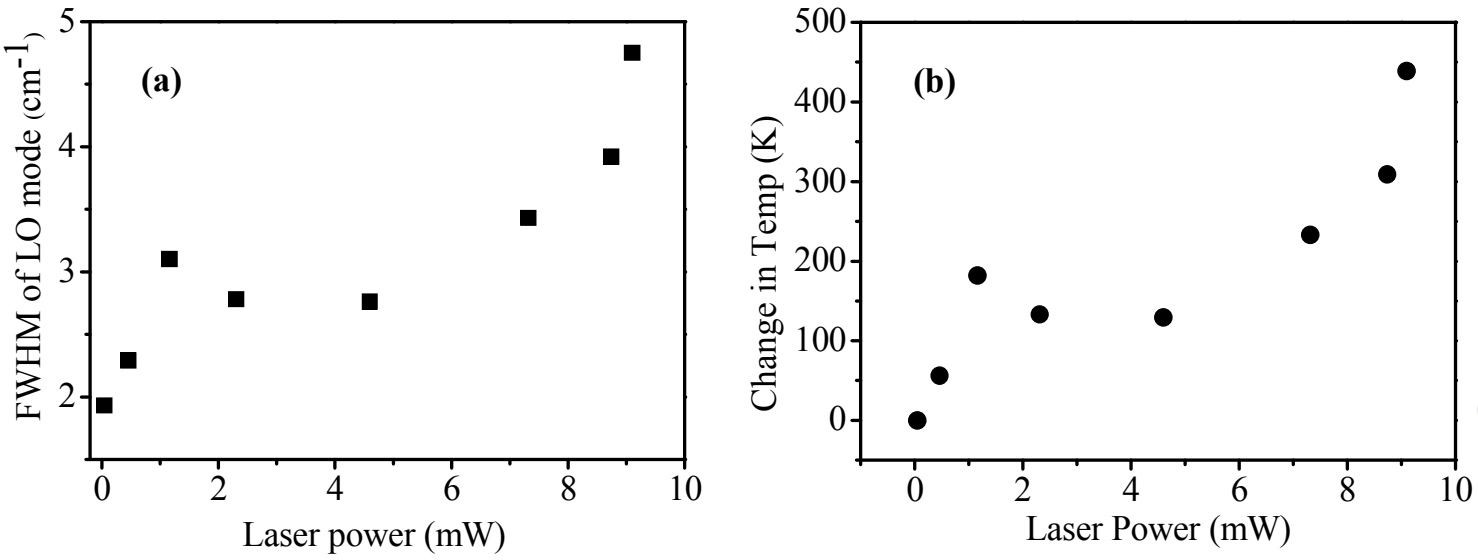

Figure 2: (a) FWHM of LO mode as a function of laser power, (b) Change of local temperature as a function of laser power obtained from experimental data.

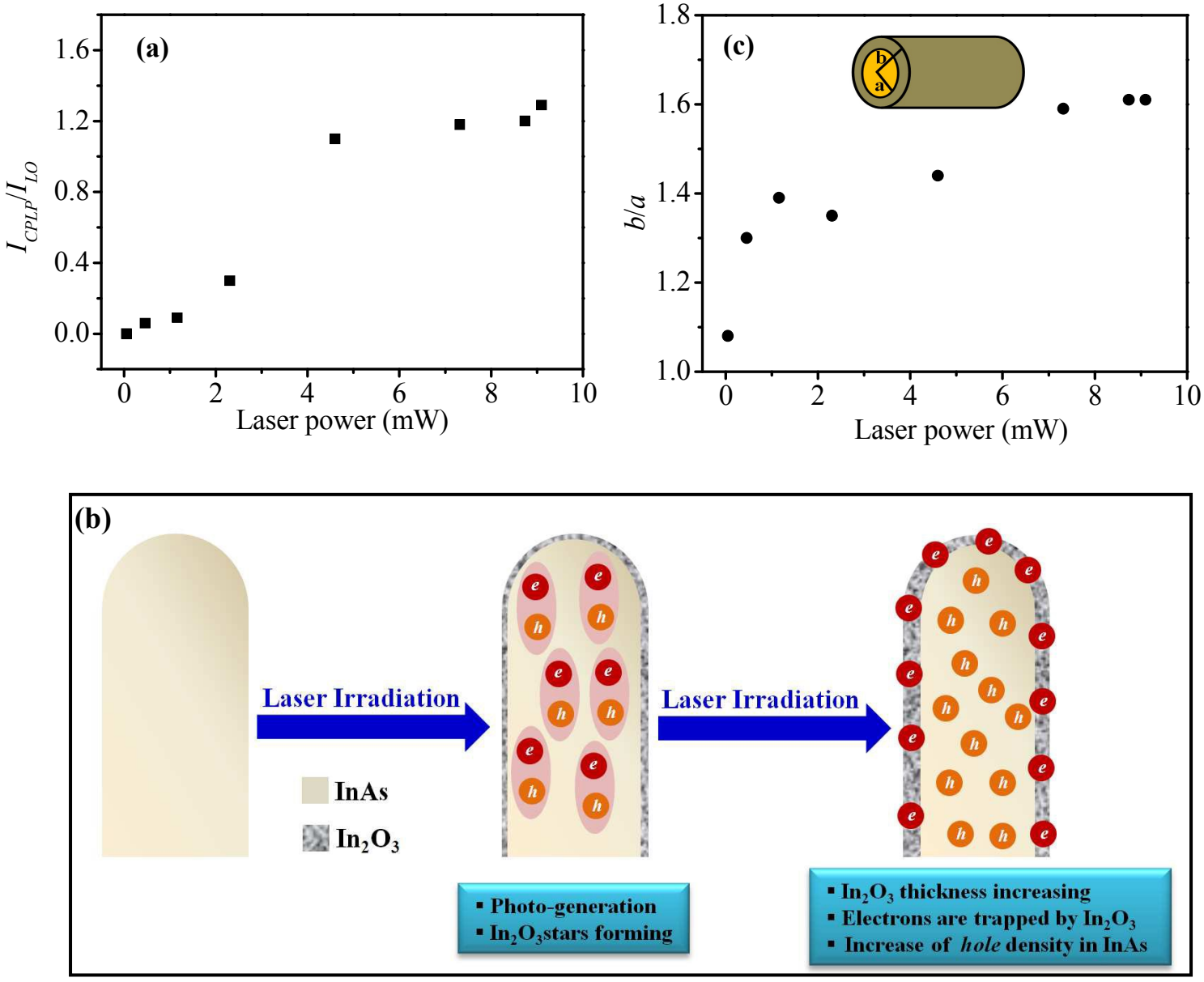

Figure 3: (a) Variation of I_{CPLP}/I_{LO} as a function of laser power, (b) Schematic representation of our proposed mechanism, (c) Variation of b/a as a function of laser power. The inset shows the schematic representation of core/shell structure.

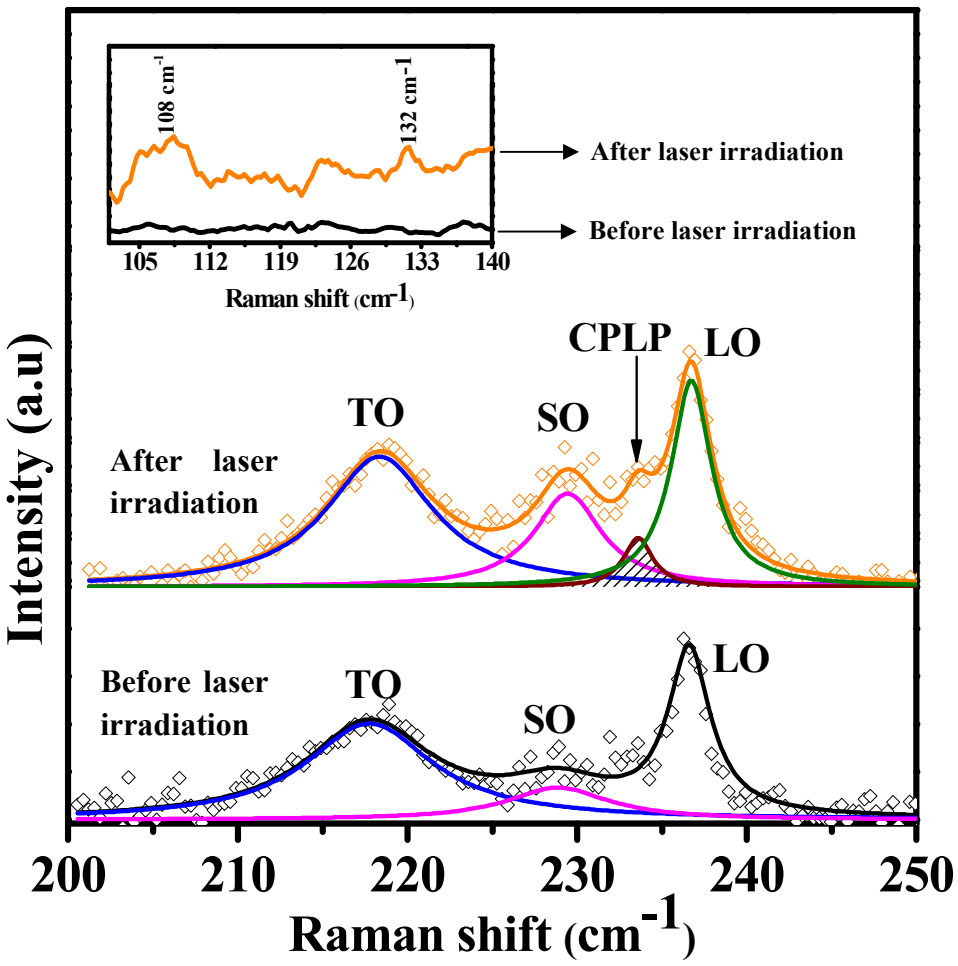

Figure 4: Raman spectra (symbols) measured with very low laser power before and after oxidation by laser irradiation in air. The spectra are fitted with multiple Lorentzian functions. Solid lines represent the fitted curves. The inset shows the same spectra within the range 100-140 cm^{-1}.

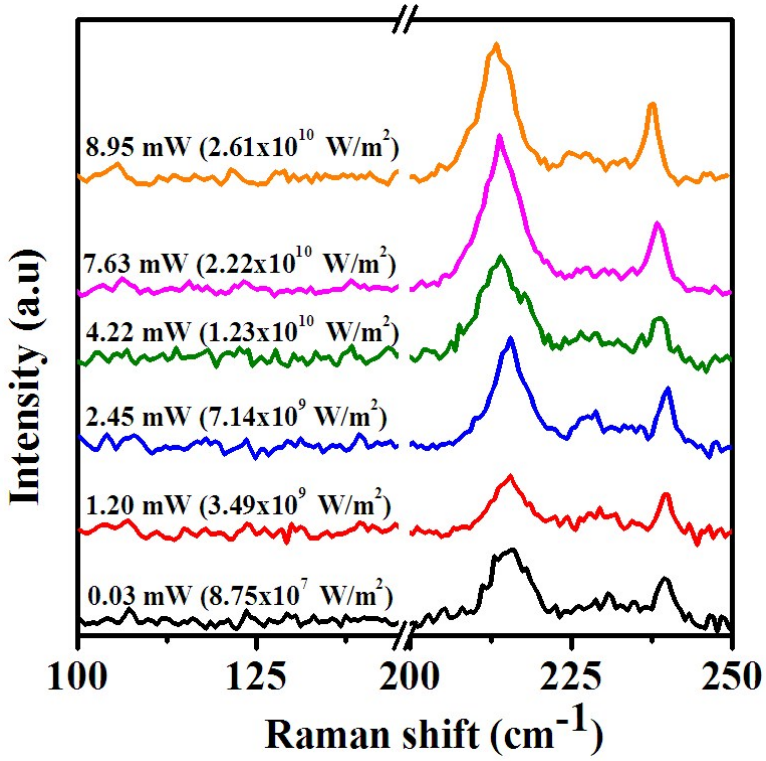

Figure 5: Raman spectra of InAs NW at different laser powers from lower (bottom) to higher (top) laser power (power density), indicated for each curve taken at vacuum (10^{-3} mbar). The individual spectra are vertically shifted for clarity.

Table1: The table contains the radius r of the non-oxidized InAs NW, values of $x=qr$, values of ω_P^2 estimated from equation (4) and the hole concentration (n_h) obtained through equation (6) at different laser powers.

Laser power (mW)	***r* (nm)**	***x***	ω_P^2	n_h (cm^{-3})
0.05	20	0.520	1.05×10^{26}	4.71×10^{17}
0.46	15.4	0.400	2.96×10^{26}	1.33×10^{18}
1.16	14.4	0.374	5.55×10^{26}	2.49×10^{18}
2.31	14.8	0.385	6.13×10^{26}	2.75×10^{18}
4.60	13.9	0.361	6.55×10^{26}	2.94×10^{18}
7.32	12.6	0.328	7.29×10^{26}	3.27×10^{18}
8.74	12.4	0.322	7.62×10^{26}	3.42×10^{18}
9.10	12.4	0.322	7.30×10^{26}	3.28×10^{18}

Table of Contents

We demonstrate the use of Raman spectroscopy as a non-contact optical tool to study the photothermal effects in nanoscale materials and tune the hole density in InAs NWs.